ASSESSING SCIENTIFIC AND INDUSTRY GRADE SWIR AIRBORNE IMAGING SPECTROMETERS FOR CH₄ MAPPING

Rebecca D. P. M. Scafutto[1]; Harald van der Werff[2]; Wim H. Bakker[2];
Freek van der Meer[2]; Carlos Roberto de Souza Filho[1]

[1] Geosciences Institute, University of Campinas
Rua Carlos Gomes, 250, 13083-855, Campinas/SP, Brazil
[2] ITC, University of Twente, Department of Earth Systems Analysis
Hengelosestraat 99, 7514 AE Enschede, The Netherlands

ABSTRACT

This study focus on the evaluation of scientific and industry-grade hyperspectral airborne sensors for the mapping of methane (CH_4) emissions in the SWIR range. An imaging dataset from areas with known CH_4 emissions was processed using the classic matched filter technique, and a new CH_4 index. The airborne sensors were evaluated based on sensor design (spectral sampling and band centers), effectiveness of image processing, and impact of the signal-to-noise ratio (SNR) on CH_4 mapping. The gas plume was mapped only in the images acquired with scientific-grade sensors. Results demonstrated that superior performance could be achieved when the position of band centers are closely located to the center of diagnostic CH_4 absorption features. The impact of SNR was examined using a noise simulation, adding white noise to simulate images with varying SNR levels. Results indicate that the noisier signal of the industry-grade sensor is probably what prevented mapping the CH_4 plume in this dataset. Simulations also demonstrated that as densest the plumes lower is the impact of SNR. Combined, results indicate that an imaging spectrometer with a scientific-grade SNR and band centers properly positioned to match the main CH_4 features would improve the mapping of CH_4 plumes with airborne sensors operating in the SWIR range.

Index Terms— *Methane, airborne, imaging spectroscopy, hyperspectral*

1. INTRODUCTION

Advances in the mapping and tracking of methane (CH_4) sources are of interest to both exploration and environmental sectors in the oil industry. Since 2007, the concentration of CH_4 in the atmosphere has been rising [1], and it is estimated that about 15-20% of the global CH_4 budget is related to the fossil fuel industry [2]. The mapping of natural (i.e. seepages) and anthropogenic (i.e. leakage) emission sources can assist in the discovery of new exploration plays, as well as in the prevention of losses in the production chain (which also assists in reducing the contributions of O&G sector to the global CH_4 budget).

Remote sensing tools have been used for the mapping and quantification of CH_4 in several scales; providing from global maps of CH_4 concentration with orbital sensors [e.g. 3], to the mapping of local point sources with high resolution imaging airborne spectrometers in the infrared range [e.g. 4, 5, 6]. In the shortwave infrared (SWIR: 1000 – 2500 nm) specifically, the detection of CH_4 relies on the spectral signature of the gas. In this range, CH_4 major absorption features are located between 2150-2500 nm [7]. Despite situated in an atmospheric window, even the strong features of the gas are week and narrow when compared to equivalent features in the TIR interval [8], making its detection difficult in the SWIR range, due to possible misclassification with background materials and noise interference [9]. To date, only the Airborne Visible and Infrared Spectrometer (AVIRIS) instruments, both Classic (AVIRIS-CL) and Next Generation (AVIRIS-NG) succeed in detecting CH_4 emissions in the SWIR [e.g. 10, 11].

In this study, we evaluate the technical specification and effectiveness in the mapping of CH_4 plumes of three high-resolution airborne imaging spectrometers. Images acquired with an industry-grade and two scientific-grade sensors were processed and analyzed, aiming to identify the key features for CH_4 mapping as well as what could be improved in the design of future airborne sensors dedicated to CH_4 detection.

2. MATERIALS & METHODS

Data from areas with know CH_4 emissions acquired with an industry-grade (IG) sensor, AVIRIS-CL and AVIRIS-NG (i.e. scientific-grade imaging spectrometers) were processed. As can be seen in Table 1, the IG sensor has more bands than AVIRIS-CL, but resembles AVIRIS-NG in spectral resolution. The imaging data from both AVIRIS-NG (ang20130623t201154) and IG sensor were acquired over two independent field experiments, performed in Casper (WY/USA) in 2013 [11] and 2010 [e.g. 12], respectively. Both experiments comprised periodic controlled releases of CH_4. The images analyzed here were acquired over the

release points gas fluxes of 23 m³/h for the IG sensor and 56.6 m³/h for AVIRIS-NG. The AVIRIS-CL image (f160112t01p00r12) was acquired in 2016, over the Aliso Canyon storage facility (leak rate of ~ 28,000 m³/h - 13).

Table 1. Specifications AVIRIS-CL[1], AVIRIS-NG[1] and IG airborne sensors

	AVIRIS-CL	AVIRIS-NG	IG sensor
Spectral Range	380 – 2500 nm	380 – 2500 nm	400 – 2450 nm
Spectral Sampling	10 nm	5 nm	6.3 nm
Number of Bands	224	427	356
SNR (SWIR)	500:1	1000:1	800:1
FOV/IFOV	34° / 1 mrad	34° / 1 mrad	24° / 1.3 mrad
Spatial Resolution of the Processed Image	6m	0.6m	0.5m

[1]Source: [11]

The methodology used to evaluate the scientific and industry-grade sensors included: (i) analysis of sensor design, (ii) image processing; and (iii) noise simulations, as described bellow.

2.1. Sensor Design

Spectral sampling and band position of each imaging spectrometer were evaluated in this step. To perform a comparable assessment, a CH_4 reference signature from HITRAN [high resolution transmittance molecular absorption database - 14] was resampled to the spectral resolution and sampling interval of each airborne sensor, using a filter-function (full width at half maximum - FWHM). The resampled spectra were also used to perform noise simulations.

2.2. Image Processing

The images acquired with the industry and scientific grade sensor were processed using two techniques: spectral index and mixed tuned matched filtering (MTMF). The CH_4 index (*CH4I*) presented by [15] was used in this study (Eq. 1). The wavelengths of the components of the equation must be adjusted to the spectral sampling of the hyperspectral sensor used (Fig.1).

$$CH_4I = \frac{MEAN\ (B_1 + B_2 + B_3)}{MEAN\ (B_4 + B_5 + B_6 + B7)} \qquad (1)$$

The matched filter technique has been used by previous authors for CH_4 mapping [e.g. 11]. By combining minimum noise fraction (MNF), matched filtering (MF) and mixture tuning (MT) the MTMF classification algorithm estimates the subpixel abundance for pure endmembers in the scene, suppressing the response of the background [16]. Here, endmembers derived from the scene were used as input reference to perform the MTMF classification.

2.3. Noise Simulation

The signal-to-noise ratio (SNR) of the hyperspectral sensors was estimated using the mean and standard deviation of 500 pixels selected over a homogeneous bright area from each image. The noise simulation was performed by adding random white noise to the images and to the resampled CH_4 HITRAN spectrum of each sensor. The noise was added with the HypPy Tools [e.g. 17].

3. RESULTS

3.1. Sensor Design

Figure 1 presents the reference (HITRAN) and resampled CH_4 spectra. Despite the main absorption features of the gas (2289, 2316, 2341, 2348, and 2370 nm) prevail in the resolution of all sensors, it is clear that features depth and definition are enhanced in the AVIRIS-NG, in comparison to the AVIRIS-NG an IG sensor spectra. This difference demonstrates that even a small increase in the spectral sampling can assist in resolving the CH_4 features. Besides, features depth and sharpness are also improved as band centers are closer to the center of CH_4 features. For that reason, features at 2289 nm and 2370 nm are better resolved in the AVIRIS-NG spectrum, while features at 2316 nm, 2341 nm and 2348 nm are better positioned in the AVIRIS-CL and IG sensor spectra.

3.2. Image Processing

The plumes were mapped in the AVIRIS-CL and AVIRIS-NG images, with both MTMF classification and *CH4I* index. However, similar results were not achieved with the image acquired with the IG sensor.

3.3. Noise Simulation

Despite similar in shape, the SNR estimated from the image acquired with the IG sensor is noisier (i.e. higher variations of values along the wavelength range) than the SNR estimated for both JPL sensors. After comparing the SNR from the image processed here (acquired on 20th August 2010) with the SNR estimated from an image acquired 2 days before (i.e. 18th August 2010) in the same area, it was inferred that this difference resulted from problems related to the radiometric calibration, once the quality of IG data is commonly high.
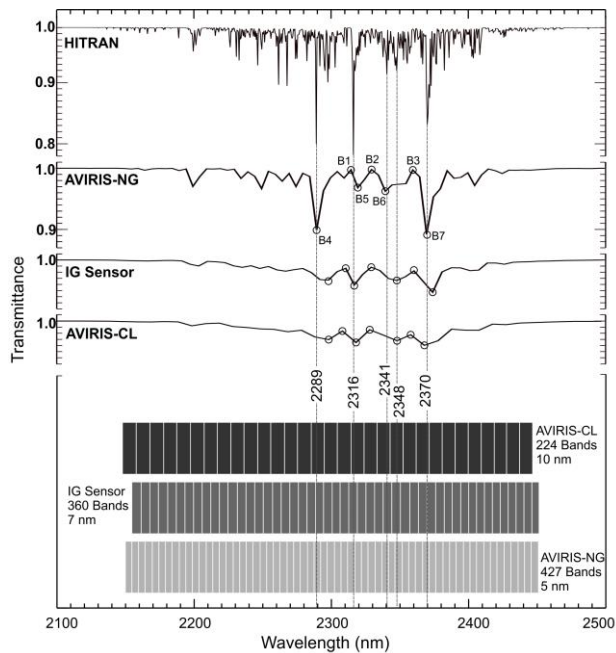
Figure 1. Location of main CH$_4$ features. The spectral signatures correspond the reference HITRAN CH$_4$ spectra and the reference resampled to the spectral resolution of AVIRIS-NG, AVIRIS-CL and IG sensor. Black circles indicate the location of bands 1-7 used as input to calculate the *CH4I*, as illustrated in the AVIRIS-NG spectrum. In the bottom, bars represent the bands and spectral sampling of each sensor, between 2150 – 2450 nm. Dashed lines indicate the position of main CH$_4$ features in relation to the band centers of the airborne sensors (adapted from [15]).

Comparing the SNRs estimated from the original images, with the SNR estimated from the images processed after noise simulation (i.e. addition of white noise), it was noticed that the number of pixels in the plume decreases as the percentage of the noise increase. Additionally, the impact of noise was minor in the AVIRIS-CL image. Due to the higher density of the mapped plume (i.e. higher gas rate), a higher percentage of noise (15%) was needed to mask the signal of the gas, compared to the other two sensors (5-7%).

4. DISCUSSION

The SNR along with high spectral sampling and resolution of AVIRIS-CL and AVIRIS-NG allows the use of these sensors for CH$_4$ mapping. On the other hand, despite having SNR and spectral sampling similar to JPL's sensors, the IG sensor failed to detect the CH$_4$ plume, demonstrating that other feature in the sensor design, such as band positioning, are as relevant as spectral resolution for CH$_4$ mapping.

Apart from the calibration issue, the band centers of the IG sensor was not well positioned in relation to the center wavelength of CH$_4$ features, as the band centers of both AVIRIS's sensors were. Although small, this displacement set the strongest CH$_4$ features to fall in the edges of the bands in the IG sensor configuration (Fig.1). For that reason,

the CH$_4$ features in the resolution of the IG sensor (7 nm sampling) are shallower, resembling the AVIRIS-CL spectra (10 nm sampling) more than the AVIRIS-NG spectra (5 nm sampling). The design of AVIRIS-NG, place the center of CH$_4$ features in more convenient wavelength, enhancing the strongest features and reducing noise sensitivity.

As regarding the impact of noise, the shallower feature depths of the CH$_4$ features in the spectra of AVIRIS-CL and the IG sensor, makes these sensors more susceptible to the increase of noise than AVIRIS-NG (in which the CH$_4$ features are narrower and deeper). Although the drop in the SNR itself has not been as significant, the variation of the signal along the wavelength makes it rougher. This irregularity of values along the SNR curve is what masks the signal of the plume as noise increase. Nevertheless, the increase in noise can be compensated by plume density. due to the significantly higher density of the plume mapped by AVIRIS-CL, the double of noise (15%) had to be added to the image to suppress the CH$_4$ plume, in comparison to the amount of noise added to the AVIRIS-NG (7%) and AVIRIS-NG resampled to IG sensor (5%) images.

Looking at the SNR estimated from the original and simulated IG images; no major change could be noticed in the roughness of the signal with the increase of noise, which highlights the poor calibration of the sensor and partially explains the failure of the IG sensor in mapping the CH$_4$ plume. Additionally to the human error in the calibration, and the fact that the sensor design is not very conducive for the detection of CH$_4$; the plume generated in the emission point of the controlled experiment may have not been dense enough to be detected by the IG sensor, even with higher gas rate (23 m^3/h).

5. CONCLUSION

This study demonstrates that high resolution alone is not enough for the detection of CH$_4$ plumes with airborne sensors in the SWIR. Aside from spectral sampling and SNR, other issues as the position of band centers in relation to the main CH$_4$ absorption features and proper radiometric calibration are also critical to resolve the signature of the gas. Additionally, the density of the plume must also be taken into consideration during image processing.

6. ACKNOWLEDGMENTS

7. REFERENCES

[1] A. J. Turner, C. Frankenberg, and E. A. Kort, "Interpreting contemporary trends in atmospheric methane," *Proceedings of the National Academy of Sciences,* vol. 116, no. 8, pp. 2805-2813, 2019.

[2] S. Schwietzke, O. A. Sherwood, L. M. Bruhwiler *et al.*, "Upward revision of global fossil fuel methane emissions based on isotope database," *Nature,* vol. 538, no. 7623, pp. 88, 2016.

[3] T. Yokota, Y. Yoshida, N. Eguchi *et al.*, "Global concentrations of CO2 and CH4 retrieved from GOSAT: First preliminary results," *Sola,* vol. 5, pp. 160-163, 2009.

[4] G. C. Hulley, R. M. Duren, F. M. Hopkins *et al.*, "High spatial resolution imaging of methane and other trace gases with the airborne Hyperspectral Thermal Emission Spectrometer (HyTES)," *Atmospheric Measurement Techniques,* vol. 9, no. 5, pp. 2393, 2016.

[5] R. Scafutto, and C. Souza Filho, "Detection of Methane Plumes Using Airborne Midwave Infrared (3–5 μm) Hyperspectral Data", *Remote Sensing,* vol. 10, no. 8, pp. 1237, 2018.

[6] D. M. Tratt, K. N. Buckland, J. L. Hall *et al.*, "Airborne visualization and quantification of discrete methane sources in the environment," *Remote Sensing of Environment,* vol. 154, pp. 74-88, 11//, 2014.

[7] J. Kamieniak, E. P. Randviir, and C. E. Banks, "The latest developments in the analytical sensing of methane," *TrAC Trends in Analytical Chemistry,* vol. 73, pp. 146-157, 2015.

[8] L. R. Brown, D. C. Benner, J.-P. Champion *et al.*, "Methane line parameters in HITRAN," *Journal of Quantitative Spectroscopy and Radiative Transfer,* vol. 82, no. 1, pp. 219-238, 2003.

[9] A. K. Ayasse, A. K. Thorpe, D. A. Roberts *et al.*, "Evaluating the effects of surface properties on methane retrievals using a synthetic airborne visible/infrared imaging spectrometer next generation (AVIRIS-NG) image," *Remote sensing of environment,* vol. 215, pp. 386-397, 2018.

[10] A. Thorpe, C. Frankenberg, A. Aubrey *et al.*, "Mapping methane concentrations from a controlled release experiment using the next generation airborne visible/infrared imaging spectrometer (AVIRIS-NG)," *Remote Sensing of Environment,* vol. 179, pp. 104-115, 2016.

[11] A. K. Thorpe, D. A. Roberts, E. S. Bradley *et al.*, "High resolution mapping of methane emissions from marine and terrestrial sources using a Cluster-Tuned Matched Filter technique and imaging spectrometry," *Remote Sensing of Environment,* vol. 134, pp. 305-318, 2013.

[12] R. D. M. Scafutto, C. R. de Souza Filho, D. N. Riley *et al.*, "Evaluation of thermal infrared hyperspectral imagery for the detection of onshore methane plumes: Significance for hydrocarbon exploration and monitoring," *International Journal of Applied Earth Observation and Geoinformation,* vol. 64, pp. 311-325, 2018.

[13] S. Conley, G. Franco, I. Faloona *et al.*, "Methane emissions from the 2015 Aliso Canyon blowout in Los Angeles, CA," *Science,* vol. 351, no. 6279, pp. 1317-1320, 2016.

[14] I. E. Gordon, L. S. Rothman, C. Hill *et al.*, "The HITRAN2016 molecular spectroscopic database," *Journal of Quantitative Spectroscopy and Radiative Transfer,* vol. 203, pp. 3-69, 2017.

[15] R. Scafutto, H. van der Werff, W. H. Bakker, F. van der Meer, C. Souza Filho, "An evaluation of airborne SWIR imaging spectrometers for CH4 mapping: Implications of band positioning, spectral sampling and noise", *International Journal of Applied Earth Observation and Geoinformation,* vol. 94, 2021 – in press.

[16] J. C. Harsanyi, and C.-I. Chang, "Hyperspectral image classification and dimensionality reduction: An orthogonal subspace projection approach," *IEEE Transactions on geoscience and remote sensing,* vol. 32, no. 4, pp. 779-785, 1994.

[17] W. Bakker, F. Van Ruitenbeek, H. Van Der Werff *et al.*, "Processing OMEGA/Mars Express hyperspectral imagery from radiance-at-sensor to surface reflectance," *Planetary and space science,* vol. 90, pp. 1-9, 2014.